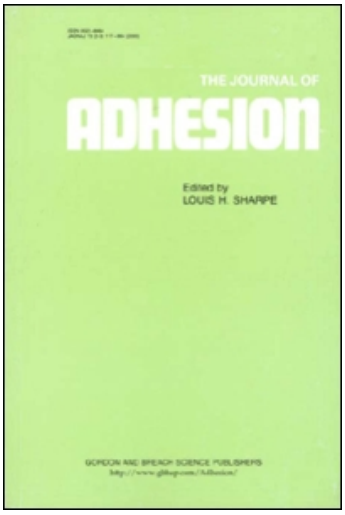


## The Journal of Adhesion

Publication details, including instructions for authors and subscription information:
http://www.informaworld.com/smpp/title~content=t713453635

# Residual Stresses in Microcomposites and Macrocomposites

H. D. Wagner[a]
[a] Department of Materials & Interfaces, The Weizmann Institute of Science, Rehovot, Israel

**To cite this Article** Wagner, H. D.(1995) 'Residual Stresses in Microcomposites and Macrocomposites', The Journal of Adhesion, 52: 1, 131 — 148
**To link to this Article: DOI:** 10.1080/00218469508015190
**URL:** http://dx.doi.org/10.1080/00218469508015190

*J. Adhesion*, 1995, Vol. 52, pp. 131–148
Reprints available directly from the publisher
Photocopying permitted by license only



# Residual Stresses in Microcomposites and Macrocomposites*

H. D. WAGNER

*Department of Materials & Interfaces, The Weizmann Institute of Science, Rehovot 76100, Israel*

*(Received February 26, 1994; in final form June 11, 1994)*

Existing models for built-in residual stresses in composite materials are reviewed and discussed. In particular, the thermal longitudinal stress present in the fiber prior to a single-fiber fragmentation experiment is studied using various model composite data. It is found that this stress is typically compressive in nature and that, quantitatively, it depends on the fiber content, the degree of undercooling, and the thermoelastic constants of the fiber and the matrix. In the case of single-fiber composites (or microcomposites), the thermal longitudinal stress present in the fiber is high enough to either induce fiber sinewave buckling (such as in E-glass/epoxy), or extensive fiber fragmentation (such as in graphite HM/polypropylene) that may then be used to measure the dependence of compressive fiber strength upon length. This has to be accounted for in quantitative models that calculate interfacial adhesion parameters using single-fiber tests, such as the fragmentation test or the microbond test. Implications for high fiber content composites (or macrocomposites) are discussed.

KEY WORDS: Residual thermal stresses; microcomposites; single fiber composites; fiber fragmentation; compressive strength of single fibers; concentric cylinders models;



## 1. INTRODUCTION

The single-fiber composite (or fragmentation) test[1-5] was invented in the mid-seventies and developed to estimate the degree of adhesion between a rigid fiber and a more ductile polymer matrix. The calculation of the interfacial shear strength ($\tau$), which reflects the extent to which the fiber and matrix constituents adhere, involves the use of the Kelly-Tyson equation.[6] This equation contains, as one of the key parameters, the tensile stress in a fiber fragment of very small length (the length obtained when the fragmentation phenomenon reaches its saturation state, of the order of a few hundreds of microns in typical polymer-based composites). Usually, all pre-existing stresses in the fiber (such as residual, thermal or fabrication stresses) are considered to be very small, and are not included in the calculations. Based on the results of recent experiments,[7-9] it has been observed that compressive fiber fragmentation may be induced during sample preparation. This implies that very large compressive stresses (several GPa) are present in the fiber prior to the fragmentation test. This "spontaneous" fiber breaking is attributed to residual thermal stresses, which are also

*One of A Collection of papers honoring Lawrence T. Drzal, the recipient in February 1994 of *The Adhesion Society Award for Excellence in Adhesion Science*, Sponsored by 3M.

responsible for the fiber buckling sometimes observed in unidirectional composites under compressive stress parallel to the fiber direction.

The objective of the present work is to review various models proposed in the literature for the calculation of residual stresses present in single-fiber composites due to cooling from a relatively high manufacturing temperature. The type of single-fiber composite, in which fiber fragmentation might arise in a fiber *before* a fragmentation test is performed, is discussed. The effect of fiber content is also addressed.

## 2. SURVEY OF MODELS

A look at the literature reveals the existence of various theoretical expressions for the principal (radial, circumferential, and longitudinal) stresses in the (cylindrical) fibers and the matrix, and at the interface between these, due to the thermal shrinkage that results from sample preparation. As will be seen, some models account for possible anisotropy of the fiber, but most do not. All schemes assume a perfect, infinitely-thin interface, except for the model of Nairn,[10] where an interphase region is included. Broadly speaking, all models can be classified in two groups, namely, (i) the schemes based on one-dimensional modelling, and (ii) the schemes based on the solution of the classical "shrink-fit" problem for concentric cylinders. The main expressions obtained from both approaches are now reviewed and discussed.



### 2.1. One-dimensional Models

Several authors consider a unidirectional composite in a state of plane stress, corresponding to thin laminates, under a thermal strain. No mechanical stresses are applied. Both the fibers and the matrix are assumed to be isotropic. The only residual stress components present in the fibers and the matrix are assumed to be the longitudinal components $\sigma_z^f$ and $\sigma_z^m$, respectively, given by

$$\sigma_z^f = (\alpha_m - \alpha_f)(T - T_{ref}) \frac{E_f}{1 + \left(\frac{\phi_f}{\phi_m}\right)\left(\frac{E_f}{E_m}\right)} \tag{1}$$

$$\sigma_z^m = -\sigma_z^f \frac{\phi_f}{\phi_m} \tag{2}$$

where $\alpha$ and $E$ are the (isotropic) coefficient of thermal expansion and Young's modulus, respectively, $\phi$ is the content by volume, with the subscripts $m$ or $f$ for the matrix or the fiber, and where $T$ is the test temperature and $T_{ref}$ the stress-free reference temperature. These equations are taken form Tsai and Hahn.[11] Possible orthotropic symmetry of the fibers and the matrix can be included[12] in these formulae by replacing $\alpha_f$ and $\alpha_m$ by $\alpha_{fL}$ and $\alpha_{mL}$, and $E_f$ and $E_m$ by $E_{fL}$ and $E_{mL}$, respectively. Identical equations are presented by Zong and Marcus,[13] and related expressions are proposed by Peters and Andersen[14] for cross-ply laminates. Note that another assumption included in the above model (as well as in most other models) is that the physical parameters ($\alpha$ and $E$) in Eqs. (1–2) are independent of temperature in the range between

$T$ and $T_{ref}$, which is not always the case. As shown by several authors,[15,16] the dependence of the elastic constants on temperature may be accounted for by replacing the temperature difference in the above equations by $dT$ and integrating between $T$ and $T_{ref}$, with the temperature-dependent elastic constants replacing those in Eq. (1). Filiou *et al.*,[17] further subdivide the temperature range into two sub-ranges for the purpose of integration, namely, between $T$ and $T_g$ and then between $T_g$ and $T_m$.

Another approximate one-dimensional model can be constructed as follows, specifically for the single fiber composite test.

*Step 1*: The fiber and the matrix components are viewed as if they were not in contact with each other. At the reference temperature (defined as above) we have

$$\varepsilon_f^{(1)} = \frac{W}{A_f E_f}$$

and

$$\varepsilon_m^{(1)} = 0$$

where $W$ is the preload and $A_f$ is the cross-sectional area of the fiber. The only strain present in the fiber at the reference temperature is due to the pre-loading weights that are sometimes fastened at both ends of the fiber prior to embeddment into the matrix (this is done to keep the fiber straight during preparation and polymerization of the matrix).

*Step 2*: The fiber and the matrix are cooled down (separately) to room temperature, producing the following strains:

$$\varepsilon_f^{(2)} = \alpha_f(T - T_{ref}) + \frac{W}{A_f E_f} \tag{3}$$

and

$$\varepsilon_m^{(2)} = \alpha_m(T - T_{ref}) \tag{4}$$

*Step 3*: The fiber and matrix are now put back into contact to form a composite. Assuming perfect bonding, the final strains at the fiber-matrix interface should be perfectly matching, thus

$$\varepsilon_f^{(3)} = \varepsilon_f^{(2)} + \delta\varepsilon_f \tag{5}$$

$$\varepsilon_m^{(3)} = \varepsilon_m^{(2)} + \delta\varepsilon_m \tag{6}$$

where $\delta\varepsilon_f$ and $\delta\varepsilon_m$ are the changes in strain of the fiber and the matrix, respectively, associated with reestablishing perfect bonding. These changes are of opposite signs, and we assume that $|\delta\varepsilon_f| \approx |\delta\varepsilon_m|$.

Our objective is to determine the residual strains in the fiber and the matrix at step 3. Recalling that there is no mechanical force applied to the composite, apart from a fiber pre-load, $W$, the following force balance pertains:

$$\varepsilon_m^{(3)} E_m \phi_m + \left(\varepsilon_f^{(3)} - \frac{W}{A_f E_f}\right) E_f \phi_f = 0 \tag{7}$$

Equation (6) shows

$$\delta\varepsilon_m \approx -\delta\varepsilon_f = \varepsilon_f^{(2)} - \varepsilon_f^{(3)} \tag{8}$$

which may be combined with Eqs. (3–4), and (6) to yield

$$\varepsilon_m^{(3)} = \alpha_m(T - T_{ref}) + \frac{W}{A_f E_f} + \alpha_f(T - T_{ref}) - \varepsilon_f^{(3)} \tag{9}$$

By insertion of Eq. (9) into Eq. (7) we obtain

$$\varepsilon_f^{(3)} = \left(\frac{W}{A_f E_f}\right)\frac{E_f \phi_f}{E_f\phi_f - E_m\phi_m} - \left[(\alpha_m + \alpha_f)(T - T_{ref}) + \frac{W}{A_f E_f}\right]\frac{E_m \phi_m}{E_f\phi_f - E_m\phi_m} \tag{10}$$

Finally, since $\sigma_f^{resid} = \varepsilon_f^{(3)} E_f$, we have the following result for the residual fiber stress:

$$\sigma_z^f = \left(\frac{W}{A_f}\right)\frac{\left(\frac{\phi_f}{\phi_m}\right)\left(\frac{E_f}{E_m}\right)}{\left(\frac{\phi_f}{\phi_m}\right)\left(\frac{E_f}{E_m}\right) - 1} - \left[(\alpha_m + \alpha_f)(T - T_{ref}) + \frac{W}{A_f E_f}\right]\frac{E_f}{\left(\frac{\phi_f}{\phi_m}\right)\left(\frac{E_f}{E_m}\right) - 1} \tag{11}$$

Later in this work, Eq. (11) will be used in the limiting case where $W = 0$ and $\phi_f \to 0$ (it will be seen that Eq. (11) is valid only at very small fiber content values, well below the value defined from the singularity in the denominator). The residual stress in the matrix is obtained from Eq. (7), rewritten as follows in terms of stress rather than strain:

$$\sigma_z^m = -\left(\sigma_z^f - \frac{W}{A_f}\right)\frac{\phi_f}{\phi_m} \tag{12}$$

These results (Eqs. (1) and (11)) will be further examined in the Discussion section.

In the one-dimensional models presented so far, the only stress components considered were the longitudinal ones. Transverse residual stresses can also be calculated by means of a more complete, three-dimensional analysis. This is made possible by means of several versions of the "shrink-fit" composite cylinder model, which are now reviewed.

### 2.2. Three-dimensional Models

Refering to Figure 1, two concentric cylinders are assembled together at a relatively high temperature, $T_{ref}$, and then cooled down to temperature $T$. The problem consists in determining the stresses that develop in the cylinders as the temperature decreases progressively, down to temperature $T$, given that they possess different elastic constants and coefficients of thermal expansion. Perfect interfacial contact is assumed. Various authors have addressed this problem, among them Poritsky,[18] Brugger,[19] Haslett and McGarry,[20] Nairn,[10] and more recently Jayaraman and Reifsnider,[21] Lawrence *et al.*,[22] and Di Landro and Pegoraro.[23] A detailed outline of the solution is presented here, following the methods of Haslett and McGarry[20] and, mostly, Nairn.[10] The work presented here is slightly more general than the previous results, as we consider both cylinders to be transversely isotropic (Nairn studied the case where only

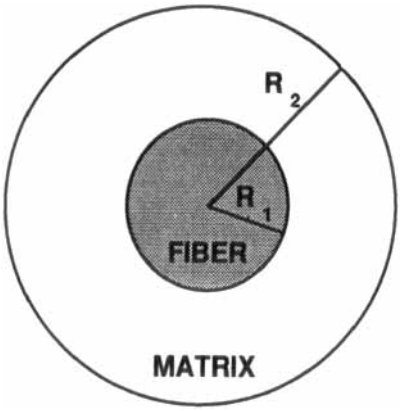


FIGURE 1 Cross section of the "shrink-fit" composite cylinder model.



the central cylinder-thus, the fiber-is transversely isotropic). In the present case, this type of anisotropy is a specialized case of orthotropy,[24] namely, the $(r, \theta)$ plane is a plane of isotropy (alternatively, one could state that the thermoelastic properties in the $r$ and $\theta$ directions are equivalent).

*i) One cylinder*: First, consider a *single* hollow cylinder with free ends, subjected to the following conditions: (i) the axial strain is constant, so that plane sections perpendicular to the axis remain planar during straining; (ii) Every cross-section perpendicular to the axis undergoes radial strains only (for example, internal and/or external pressurization). This is a classical elasticity problem, and for a linear elastic, isotropic cylinder under internal pressure $P_i$ and external pressure $P_0$, the textbook solution[25-28] is

$$\sigma_{rr} = -P_i \frac{\left(\frac{b}{r}\right)^2 - 1}{\left(\frac{b}{a}\right)^2 - 1} - P_0 \frac{1 - \left(\frac{a}{r}\right)^2}{1 - \left(\frac{a}{b}\right)^2} \tag{13}$$

$$\sigma_{\theta\theta} = P_i \frac{\left(\frac{b}{r}\right)^2 + 1}{\left(\frac{b}{a}\right)^2 - 1} - P_0 \frac{1 + \left(\frac{a}{r}\right)^2}{1 - \left(\frac{a}{b}\right)^2} \tag{14}$$

$$\sigma_{zz} = \xi \text{ (a constant)} \tag{15}$$

where $\sigma_{rr}$, $\sigma_{\theta\theta}$, and $\sigma_{zz}$ are the radial, hoop and longitudinal stresses at a distance $r$ from the symmetry axis, and a and $b$ are the internal and external radii of the cylinder, respectively.

*ii) Two cylinders*: The next step is to consider two concentric cylinders, where the internal cylinder (the fiber) is solid rather than hollow, and where both cylinders are

transversely isotropic, rather than isotropic. Following Lekhnitskii,[24] and including thermal strain effects, the strain-stress relationship for transversely isotropic materials has the form (in cylindrical coordinates):

$$\begin{pmatrix} \varepsilon_{rr} \\ \varepsilon_{\theta\theta} \\ \varepsilon_{zz} \end{pmatrix} = \begin{bmatrix} \frac{1}{E_r} & -\frac{\nu_{\theta r}}{E_r} & -\frac{\nu_{zr}}{E_z} \\ -\frac{\nu_{\theta r}}{E_r} & \frac{1}{E_r} & -\frac{\nu_{zr}}{E_z} \\ -\frac{\nu_{zr}}{E_z} & -\frac{\nu_{zr}}{E_z} & \frac{1}{E_z} \end{bmatrix} \begin{pmatrix} \sigma_{rr} \\ \sigma_{\theta\theta} \\ \sigma_{zz} \end{pmatrix} + \begin{pmatrix} \alpha_r \\ \alpha_r \\ \alpha_z \end{pmatrix} \Delta T \tag{16}$$

where $\nu$ and $E$ are Poisson's ratio and Young's modulus, respectively, and $\Delta T = T - T_{\text{ref}}$ (Eq. (16) is also called the Duhamel-Neumann relationships). As necessary, there are 4 independent elastic constants and two thermal expansion coefficients. Transverse isotropy is a convenient case since it can be shown that the form of the stresses in the cylinders is the same as for the isotropic case,[10] whereas this is not true for other specialized cases of orthotropy.

For the fiber (the internal cylinder) the internal pressure and internal radius are zero. Eqs. (13)–(15) become:

$$\sigma_{rr}^f = \sigma_{\theta\theta}^f = A^f \tag{17}$$

$$\sigma_{zz}^f = C^f \tag{18}$$

where $A^f$ and $C^f$ are constants. On the other hand, the pressure on the outer surface of the external cylinder (the matrix) is zero (in our original thermal stress problem) and Eqs. 13–15 become:

$$\sigma_{rr}^m = A^m + B^m \left(\frac{R_1}{r}\right)^2 \tag{19}$$

$$\sigma_{\theta\theta}^m = A^m - B^m \left(\frac{R_1}{r}\right)^2 \tag{20}$$

$$\sigma_{zz}^m = C^m \tag{21}$$

where $A^m$, $B^m$ and $C^m$ are constants, and the notations for the internal and external radii are now $R_1$ and $R_2$, instead of $a$ and $b$. Thus, the problem is reduced to the determination of the 5 constants $A^f$, $C^f$, $A^m$, $B^m$ and $C^m$. The radial stress boundary conditions are associated with continuity of tractions at interfaces:

$$\sigma_{rr}^m = 0 \quad \text{at} \quad r = R_2 \tag{22}$$

$$\sigma_{rr}^m = \sigma_{rr}^f \quad \text{at} \quad r = R_1 \tag{23}$$

A force balance in the longitudinal direction yields

$$\sigma_{zz}^m \phi_m + \sigma_{zz}^f \phi_f = 0 \tag{24}$$

where $\phi_f = (R_1/R_2)^2$, and $\phi_m = 1 - \phi_f$. Using Eqs. (17)–(21), the conditions (22)–(24) yield

$$B^m = -\frac{A^m}{\phi_f} \tag{25}$$

$$A^f = -A^m \frac{\phi_m}{\phi_f} \tag{26}$$

$$C^f = -C^m \frac{\phi_m}{\phi_f} \tag{27}$$

These expressions reduce the number of unknowns to only two, namely, $A^m$ and $C^m$. These latter can be determined by applying the strain-stress relations (16) with the interfacial no-slip conditions:

$$\varepsilon_{zz}^f = \varepsilon_{zz}^m \quad \text{at } r = R_1 \tag{28}$$

and $u_r^f = u_r^m$ at $r = R_1$ (where the $u$ denote the displacements), which, since $u_r = r\varepsilon_{\theta\theta}$, is equivalent to

$$\varepsilon_{\theta\theta}^f = \varepsilon_{\theta\theta}^m \quad \text{at } r = R_1 \tag{29}$$

The no-slip conditions (28) and (29), combined with the thermoelastic relations (16), yield two simultaneous equations with two unknowns:

$$\begin{aligned} A^m K_1 + C^m K_2 + M_1(T - T_{ref}) &= 0 \\ A^m K_3 + C^m K_4 + M_2(T - T_{ref}) &= 0 \end{aligned} \tag{30}$$

where:

$$K_1 = 2\left(\frac{\nu_{zr}^m}{E_z^m} + \frac{\nu_{zr}^f}{E_z^f}\frac{\phi_m}{\phi_f}\right) \tag{31}$$

$$K_2 = -\left(\frac{1}{E_z^m} + \frac{1}{E_z^f}\frac{\phi_m}{\phi_f}\right) \tag{32}$$

$$K_3 = -\left[\frac{1 - \nu_{\theta r}^f}{E_r^f}\frac{\phi_m}{\phi_f} + \frac{1 - \nu_{\theta r}^m}{E_r^m} + \frac{1 + \nu_{\theta r}^m}{E_r^m}\frac{1}{\phi_f}\right] \tag{33}$$

$$K_4 = \frac{\nu_{zr}^m}{E_z^m} + \frac{\nu_{zr}^f}{E_z^f}\frac{\phi_m}{\phi_f} \tag{34}$$

and

$$M_1 = (\alpha_z^f - \alpha_z^m) \tag{35}$$

$$M_2 = (\alpha_r^f - \alpha_z^m) \tag{36}$$

If the matrix is isotropic, the $K_i$'s reduce to the corresponding matrix elements previously given by Nairn (see Table 3 in Reference 10).

Solving Eq. (30) yields:

$$A^m = -\frac{K_4 M_1 - K_2 M_2}{K_1 K_4 - K_2 K_3}(T - T_{ref}) \tag{37}$$

$$C^m = -\frac{K_1 M_2 - K_3 M_1}{K_1 K_4 - K_2 K_3}(T - T_{ref}) \tag{38}$$

By inserting these results into Eqs. (25)–(27), the residual thermal stresses in both the fiber and the matrix may be determined from Eqs. (17)–(21). Haslett and McGarry[20] developed a similar model, but assumed from the onset that the fiber content was negligible compared with the matrix content. Moreover, they performed their calculations specifically for E-glass/epoxy only. Changing their notations and reworking their equations in a different way, their result may be presented in the following more general manner:

$$\sigma_z^f = \left[\frac{E_z^f}{1 - 2\left(\frac{\nu_f}{\kappa}\right)}\right](T - T_{ref})(\alpha_z^m - \alpha_z^f) \tag{39}$$

and

$$\sigma_r^f = \frac{\sigma_z^f}{\kappa} \tag{40}$$

for the longitudinal and radial stresses in the fiber, respectively, and where

$$\kappa = 1 + \left(\frac{E_z^f}{E_z^m}\right)\left(\frac{1 + \nu_m}{1 + \nu_f}\right) \tag{41}$$



## 3. DISCUSSION

We now compare the results obtained by means of the various models surveyed above, using data for E-glass/epoxy and HM-graphite/polypropylene. Those materials are taken as representative of, respectively, a conventional thermoset-based composite with an isotropic fiber, and a thermoplastic-based composite with a highly anisotropic fiber. Data for these materials are presented in Table I. Of particular importance is the comparison between the residual stresses present in composites with low fiber volume fraction (microcomposites) and those present in composites with high fiber volume fraction (macrocomposites), which will be amply illustrated.

The residual, thermal stress in the fiber induced by cooling an E-glass fiber/epoxy single-fiber composite is shown in Figure 2(a), as a function of the degree of undercooling relative to the stress-free temperature level, using the four models reviewed in Section 2. We focus on microcomposite specimens that have dimensions representative of those used in fragmentation tests. In such an E-glass/epoxy microcomposite, the

TABLE I

Thermomechanical data for E-glass/epoxy and HM-graphite/polypropylene (i) E-glass/epoxy:

| | E-glass | Epoxy |
|---|---|---|
| Young's modulus $E_z$[GPa] | 72.5 | 4.0 |
| Young's modulus $E_r$[GPa] | 72.5 | 4.0 |
| Poisson's ratio $\nu_{zr}$ | 0.22 | 0.4 |
| Poisson's ratio $\nu_{\theta r}$ | 0.22 | 0.4 |
| Thermal expansion coefficient $\alpha_z[10^{-6}\,C^{-1}]$ | 5.04 | 6.30 |
| Thermal expansion coefficient $\alpha_r[10^{-6}\,C^{-1}]$ | 5.04 | 6.30 |
| Fiber Radius [$\mu$m] | 8.5 | |

(ii) HM-graphite/polypropylene:

| | HM-graphite | Polypropylene |
|---|---|---|
| Young's modulus $E_z$[GPa] | 750.0 | 4.0 |
| Young's modulus $E_r$[GPa] | 15.0 | 4.0 |
| Poisson's ratio $\nu_{zr}$ | 0.22 | 0.3 |
| Poisson's ratio $\nu_{\theta r}$ | 0.25 | 0.3 |
| Thermal expansion coefficient $\alpha_z[10^{-6}\,C^{-1}]$ | −1.50 | 110.0 |
| Thermal expansion coefficient $\alpha_r[10^{-6}\,C^{-1}]$ | 10.0 | 110.0 |
| Fiber Radius [$\mu$m] | 5.0 | |



typical fiber content by volume is 0.0003 and corresponds to concentric cylinders of 17 and 980 $\mu$m diameters, respectively, for the fiber and the matrix. Figure 2(b) shows the same plot for a graphite HM/polypropylene microcomposite. Again, we assumed a fiber volume fraction of 0.0003, which, in this case, corresponds to concentric cylinders of 10 and 580 $\mu$m diameters, respectively, for the fiber and the matrix. As seen, for both types, all models are in close agreement with each other. Note the order of magnitude difference between the fiber compressive stresses induced in the E-glass/epoxy (up to $\sim 0.5$ GPa) and graphite/polypropylene (up to $\sim 12$ GPa!) composites. We elaborate on this issue later in this Section.

In a macrocomposite (fiber content of 0.5), the differences between the two types of composite are much less pronounced, as seen in Figure 3(a) and 3(b), and the theoretical models are still in good agreement with each other. Figure 3 only shows the models of Hahn-Tsai (Eq. (1), and Nairn (Eq. (18)), as these are the most reliable (as we will see). Also, the longitudinal compressive stress induced in the fiber, for both types of macrocomposites, is now of the order of a few tens of MPa, significantly lower than in the microcomposites.

The dependence on fiber content is illustrated more clearly in Figure 4 for (E-Glass/epoxy) and 5 (for graphite/polypropylene). These reveal that the simple model proposed here (Eq. (11)), as well as the model of Haslett and MacGarry (Eq. (39)), are

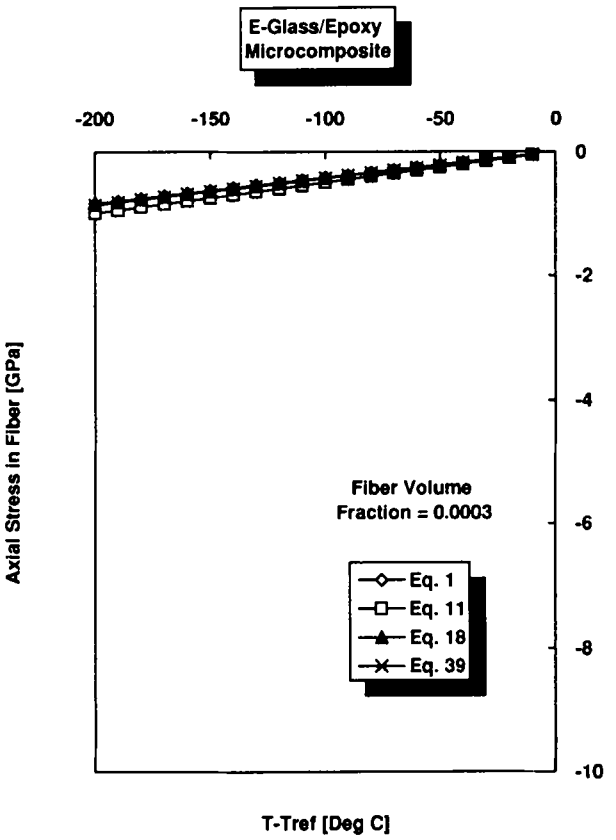


FIGURE 2 *Microcomposites*: Comparison of models for the longitudinal compressive stress induced in: (a) an E-glass fiber, by cooling a surrounding matrix of epoxy [material data are given in Table I, the fiber content by volume is 0.0003 and corresponds to concentric cylinders of 17 and 980 $\mu$m diameters, respectively, for the fiber and the matrix];

valid only at very low fiber content, thus for microcomposites only. The only models that seem valid (and are definitely consistent with each other) in the full range of fiber contents are those of Hahn and Tsai (Eq. (1)) and Nairn (Eq. (18)). For E-glass/epoxy (Figure 4), the value of $\Delta T$ was taken as $-60$°C, starting from a curing temperature of about 80°C down to room temperature, whereas for graphite/polypropylene (Figure 5), $\Delta T$ was set at $-140$°C, starting from an isothermal crystallization temperature of about 140°C down to 0°C (quenching in ice). As clearly seen, in both cases the longitudinal compressive stress in the fiber is large (a full calculation of all stresses in the fiber and the matrix using Nairn's model shows that it is in fact the largest of all stresses):

1. In E-glass, Figure 4, the compressive stress in a microcomposite with 0.0001 fiber content is of the order of $-250$ MPa, which is about 7 percent of the compressive strength of (soda-lime) glass,[29] a level which is not negligible and might be

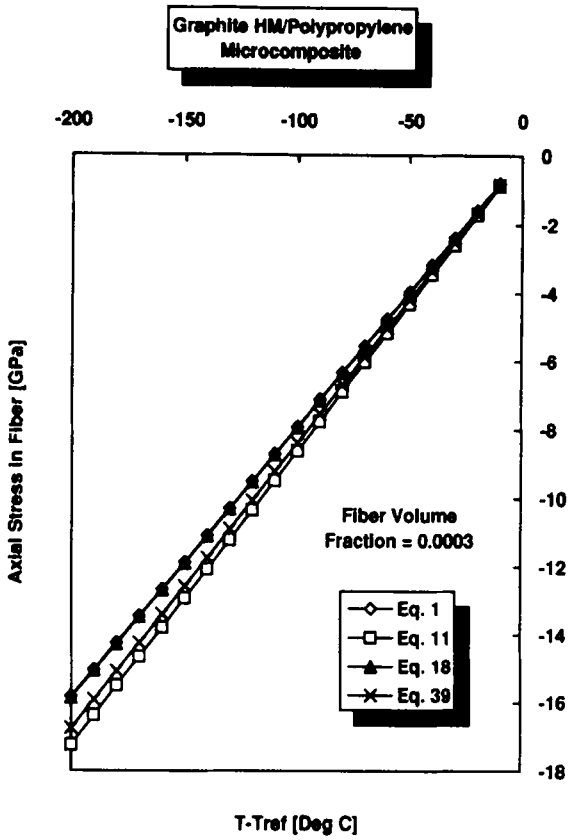


FIGURE 2 (b) A pitch-based, high-modulus graphite fiber, by cooling a surrounding matrix of polypropylene [material data are given in Table I, the fiber content by volume is 0.0003 and corresponds to concentric cylinders of 10 and 580 $\mu$m diameters, respectively, for the fiber and the matrix].

responsible for sinewave buckling of the fiber that is sometimes observed in E-glass/epoxy.

2. In graphite HM, Figure 5, the compressive stress in a microcomposite with 0.0001 fiber content is of the order of $-12$ GPa (in more physical terms, this represents a pressure in the fiber of more than 100,000 atmospheres!). For comparison, the compressive strength of high-modulus, pitch-based fibers varies between 0.5 and 1 GPa, depending on the fiber type and measurement method.[30,31] This means that the fiber will be fractured in many sites along its length due to cooling stresses, as is indeed observed (Figure 6). This provides an experimental tool to apply large compressive stresses in fibers and measure the dependence of compressive fiber strength upon fiber length.[7-9]

Important consequences of these observations are as follows:

- The single fiber fragmentation test must account for residual stresses in the fiber if an accurate calculation of the interfacial stress transfer (*via* the much used

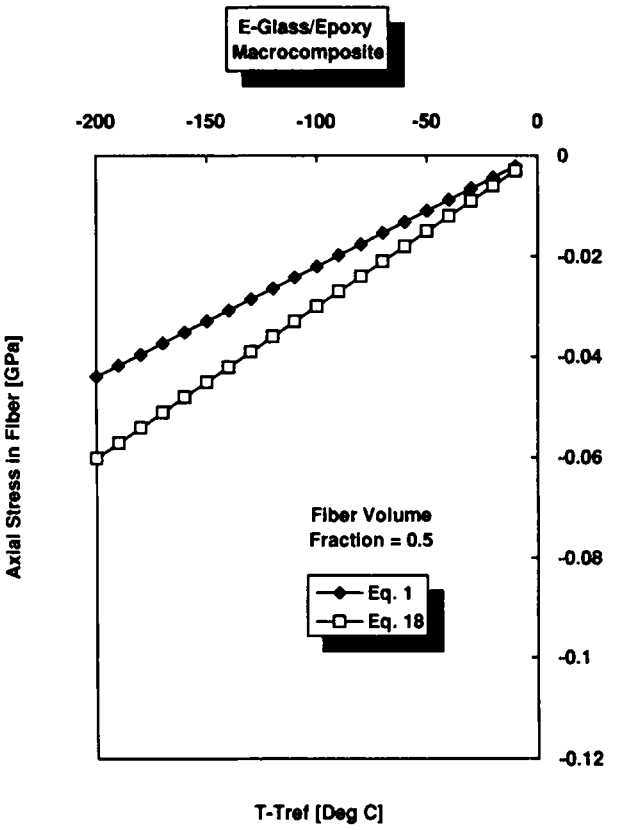


FIGURE 3 *Macrocomposites*: Comparison of models for the longitudinal compressive stress induced in: (a) an E-glass fiber, by cooling a surrounding matrix of epoxy [material data are given in Table I, the fiber content by volume is 0.5 and corresponds to concentric cylinders of 17 and 24 $\mu$m diameters, respectively, for the fiber and the matrix].



interfacial shear strength) is to be performed. This calculation is normally done by means of a Kelly-Tyson approach, which includes the strength of a short fiber fragment as one of its parameters. This strength is normally not directly accessible and thus, (i) either one extrapolates from the strength of larger fibers, a procedure which is extremely time-consuming and somewhat inaccurate, or (ii) one performs a continuously-monitored test by which the strength of the fiber fragments is measured as a function of decreasing fiber length, a procedure which is very rapid, and provides *in situ* data (unlike the previous one). It is in this latter case that one has to include thermal stress effects in the fiber.

- The stress state in a microbond test is largely modified by the presence of inhomogeneous cooling stresses in the polymeric droplet, and in the embedded portion of the fiber. These stresses must be accounted for in the calculation of the interfacial shear strength.

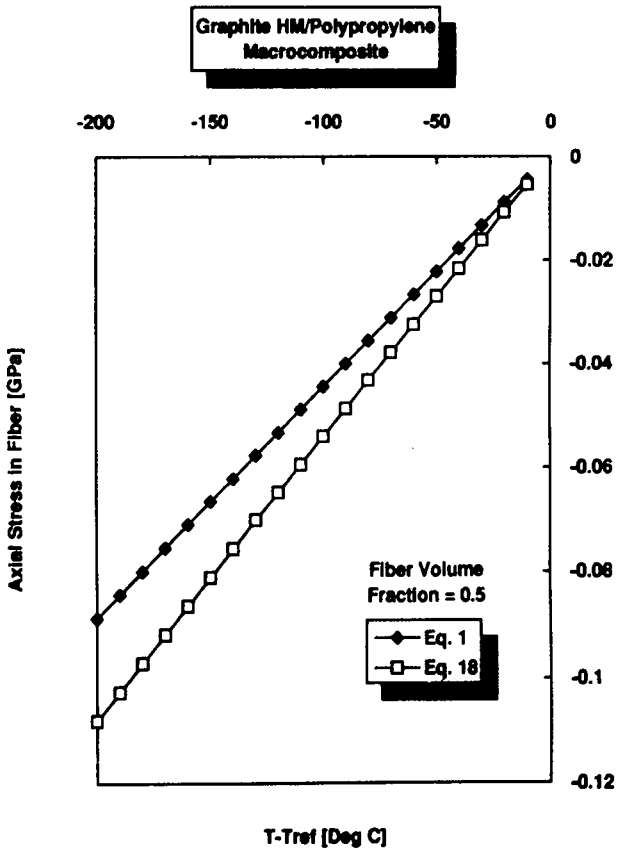


FIGURE 3 (b) A pitch-based, high-modulus graphite fiber, by cooling a surrounding matrix of polypropylene [material data are given in Table I, the fiber content by volume is 0.5 and corresponds to concentric cylinders of 10 and 14 $\mu$m diameters, respectively, for the fiber and the matrix].

A further point, which we now address, is the role of the longitudinal Young's modulus of the fiber. The strongest effects are usually observed with anisotropic, high modulus fibers and, therefore, we focus on pitch-based graphite. It is readily demonstrated that the effect of Young's modulus on the residual compressive stress in the fiber is significant only in microcomposites (Figure 7(a)), and may be neglected in macrocomposites (Figure 7(b)). Indeed, in the latter case, too little matrix is involved to induce any significant compression in the fiber, whatever its Young's modulus.

A final word concerning the effect of matrix anisotropy. Only the extended version of Nairn's model, as presented here, is able to distinguish such an effect because it includes the full set of elastic constants of the matrix. In this case, using graphite HM/polypropylene, the effect is found to be very small if the ratio of matrix Young's moduli, $E_z^m/E_r^m$, is varied by changing $E_r^m$, and is found to be moderate if the ratio is varied by changing $E_z^m$.

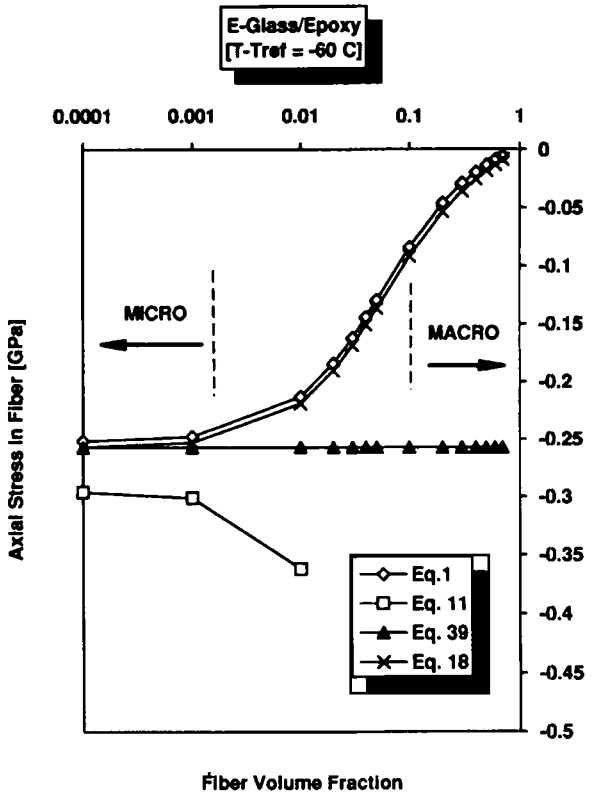


FIGURE 4 Longitudinal compressive cooling stress induced in an E-glass fiber embedded in a matrix of epoxy, as a function of fiber content. Undercooling $\Delta T$ is $-60°C$. The regions corresponding to microcomposites and macrocomposites are arbitrarily set at 0.1 percent and below, and 10 percent and above, respectively, the data in between corresponding to a transition region.



## 4. CONCLUSIONS

The major models for residual thermal stresses in composite materials were reviewed and discussed. In particular, the models of Hahn and Tsai,[11,12] and of Nairn,[10] were found to be in close agreement and are probably the most reliable. However, only Nairn's model is able to account for all stresses in both phases. The thermal longitudinal stress present in the fiber prior to a single-fiber fragmentation experiment was studied using various model composite data. It is found that, for composites made of brittle fibers within a ductile matrix, this stress is typically compressive in nature, and that, quantitatively, it depends on the fiber content, the degree of undercooling, and the thermoelastic constants of the fiber and the matrix. In the case of single-fiber composites (or microcomposites), the thermal longitudinal stress present in the fiber is high enough to induce either fiber sinewave buckling (such as in E-glass/epoxy), or extensive fiber fragmentation (such as in graphite HM/polypropylene). In the latter case, the compressive stress in the fiber is of the order of 100,000 atmospheres, which leads to the

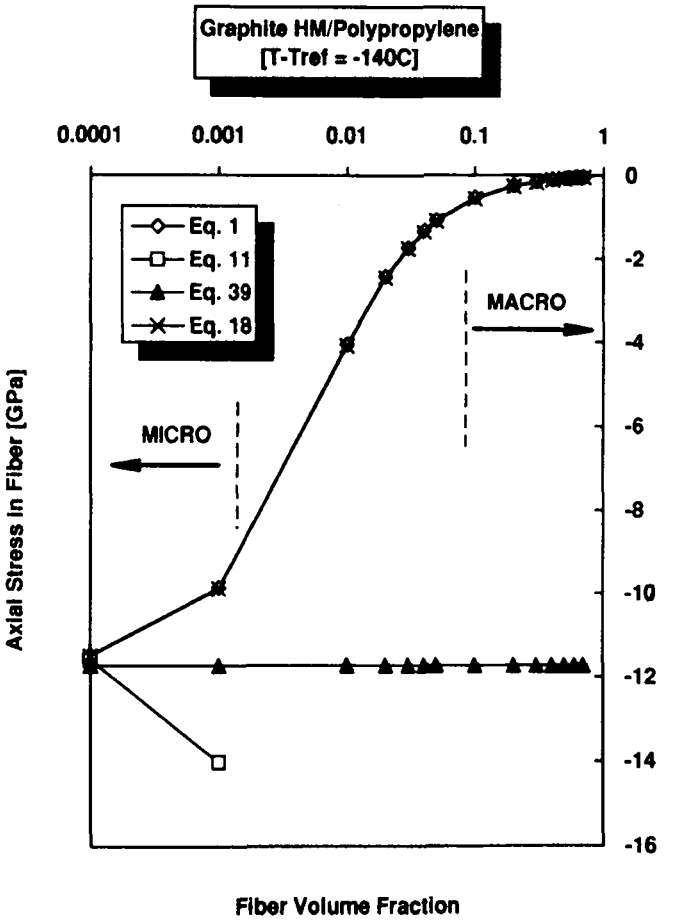


FIGURE 5 Longitudinal compressive cooling stress induced in a graphite HM fiber embedded in a matrix of polypropylene, as a function of fiber content. Undercooling $\Delta T$ is $-140°C$. The regions corresponding to microcomposites and macrocomposites are arbitrarily set at 0.1 percent and below, and 10 percent and above, respectively, the data in between corresponding to a transition region.

possibility of using, in some cases, this technique (cooling of a matrix around a thin second phase) to create very large compressive stresses in the second phase. This can be used to measure the dependence of compressive fiber strength upon fiber length.[7-9] The present work clearly shows that it is important to account for residual stresses in the fiber in order to extract valid stress transfer data from single-fiber composite (or fragmentation) tests, which are widely used to measure interfacial properties in composites. This is normally done by means of a Kelly-Tyson approach, which includes the strength of a short fiber fragment as one of its parameters. If this strength is to be measured by continuous monitoring (by which the strength of the fiber fragments is measured as a function of decreasing fiber length), one has to include thermal stress effects in the fiber. In a microbond test, the stress state in the fiber is largely modified by

FIGURE 6 Optical microscope viewing of spontaneous single fiber compressive fragmentation in HM-graphite/polypropylene, resulting from the build-up of residual thermal stresses from sample quenching. The fiber diameter is 10 $\mu$m. The glow around the fiber edges is due to the simultaneous use of transmitted and reflected light, for better viewing of the fiber breaks.

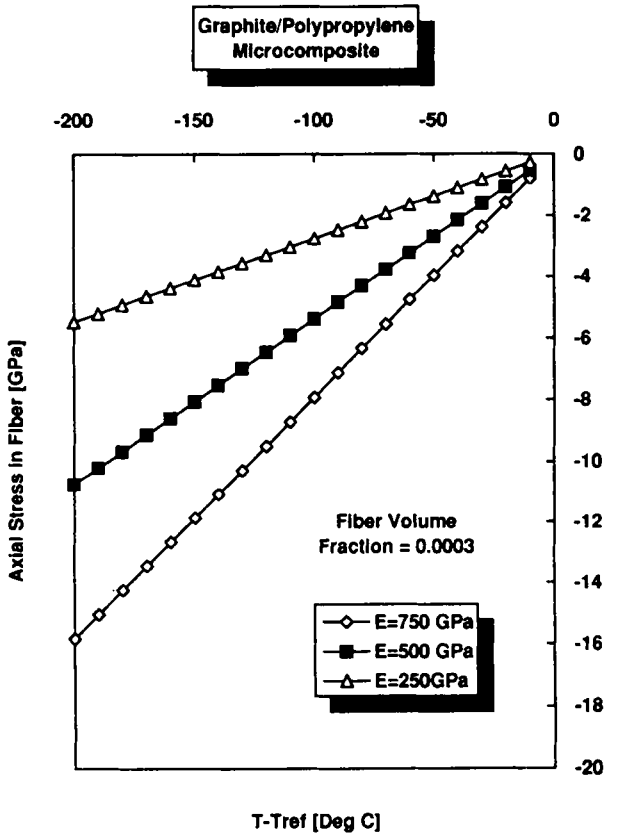


FIGURE 7 Effect of the fiber longitudinal Young's modulus on the longitudinal compressive cooling stress in the fiber. The three fiber moduli employed correspond to low, medium, and high modulus graphite. The matrix is polypropylene. (a) Results for a typical microcomposite (fiber content of 0.0003);

the presence of inhomogeneous cooling stresses in the polymeric droplet, and in the embedded portion of the fiber, and thus, again, one has to include thermal stress effects. Implications of the results for single-fiber composites relative to high fiber content composites were discussed. Finally, one must be cautious in applying the above

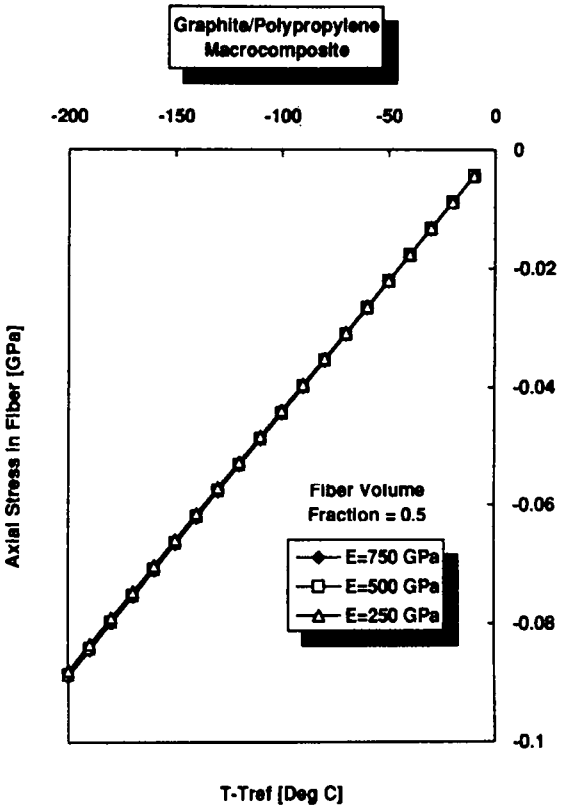


FIGURE 7 (b) Results for a typical macrocomposite (fiber content of 0.5).



theoretical models since the effect of temperature and the possible effects of cooling rate, on the various thermoelastic constants, have not been accounted for.

## Acknowledgements

This research was supported by The Basic Research Foundation administered by the Israel Academy of Sciences and Humanities. Stimulating discussions with S. Ling, J. Nairn, D. Srolovitz, G. Marom and J. Wood are acknowledged.

## References

1. W. A. Fraser, F. H. Ancker, A. T. DiBenedetto, *Proc. 30th Conf. SPI Reinforced Plastics Div.*, Section 22-A (1975).
2. L. T. Drzal, M. J. Rich, J. D. Camping, W. J. Park, *Proc. 35th Annual Technical Conf. SPI Reinforced Plastics Div.*, Section 20-C (1980)
3. A. N. Netravali, R. B. Henstenburg, S. L. Phoenix, P. Schwartz, *Polym. Composites* **10**, 226 (1989).
4. H. D. Wagner, A. Eitan, *Appl. Phys. Lett.* **56** (20), 1965 (1990).
5. B. Yavin, H. E. Gallis, J. Scherf, A. Eitan, H. D. Wagner, *Polym. Composites* **12**, 436 (1991).
6. A. Kelly, W. R. Tyson, *J. Mechanics and Phys. Solids* **13**, 329 (1965).

7. H. D. Wagner, C. Migliaresi, A. H. Gilbert, G. Marom, *J. Mater. Sci.* **27**, 4175 (1992).
8. S. Incardona, C. Migliaresi, H. D. Wagner, A. H. Gilbert, G. Marom, *Composites Sci. and Technol.* **47**, 43 (1993).
9. H. D. Wagner, J. Wood, G. Marom, *Adv. Composites Lett.* **2** (5), 173 (1993).
10. J. A. Nairn, *Polym. Composites* **6** (2), 123–130 (1985).
11. S. W. Tsai, H. T. Hahn, *Introduction to Composite Materials* (Technomic Publ. Co., Inc. Westport, CT, 1980), p. 404.
12. H. T. Hahn, *J. Composite Mater.* **10**, 266 (1976).
13. G. Zong, H. L. Marcus, *Scripta Metalurgica et Materialia* **29**, 85 (1993).
14. P. W. M. Peters, S. I. Andersen, *J. Composite Mater.* **23**, 944 (1989).
15. J. A. Nairn, P. Zoller, *J. Mater. Sci.* **20**, 355 (1985).
16. R. J. Young, R. J. Day, M. Zakikhani, I. M. Robinson, *Composite Sci. and Technol.* **34**, 243 (1989).
17. C. Filiou, C. Galiotis, D. N. Batchelder, *Composites* **23** (1), 28 (1992).
18. H. Poritski, *Physics* **5**, 406 (1934).
19. K. Brugger, *Appl. Optics* **10**, (2), 437 (1971).
20. W. H. Haslett, F. J. McGarry, *Proc. 17th Ann. Meeting Reinf. Plast. Div.*, SPI, Section 14-D (1962).
21. K. Jayaraman, K. L. Reifsnider, *Composite Sci. and Technol.* **47**, 119 (1993).
22. C. W. Lawrence, G. A. D. Briggs, C. B. Scruby, J. R. R. Davies, *J. Mater. Sci.* **28**, 3635 (1993).
23. L. Di Landro, M. Pegoraro, *Interfacial Phenomena in Composite Materials '91*, Proc. Second Intern. Conf., 17–19 Sept. 1991, Leuven, Belgium, I. Verpoest, F. Jones, Eds. (Butterworth-Heinemann Ltd, 1991), pp. 93–96.
24. S. G. Lekhnitskii, *Theory of Elasticity of an Anisotropic Elastic Body* (Holden-Day, San Francisco, 1963), p. 66.
25. S. Timoshenko, *Strength of Materials, Part II* (D. Van Nostrand Co, New York, 1930), pp. 528–536.
26. A. S. Saada, *Elasticity: Theory and Applications* (Pergamon Unified Engineering Series, New York, 1974), pp. 323–329.
27. J. Prescott, *Applied Elasticity* (Dover, New York, 1946), pp. 326–332.
28. R. V. Southwell, *An Introduction to the Theory of Elasticity for Engineers and Physicists* (Oxford Univ. Press, London 1941), pp. 391–411.
29. J. O. Outwater, D. J. Gerry, *J. Appl. Phys.* **38**, 893 (1967).
30. G. J. Hayes, D. D. Edie, J. M. Kennedy, *J. Mater. Sci.* **28**, 3247 (1993).
31. M. G. Dobb, D. J. Johnson, C. R. Park, *J. Mater. Sci.* **25**, 829 (1990).